X-ray Absorption Spectroscopy Study of FeCo−SiO2 Nanocomposites Prepared by the Sol−Gel Method

Anna Corrias,*,† Maria F. Casula,† Guido Ennas,† Sergio Marras,† Gabriele Navarra,† and Gavin Mountjoy‡

Dipartimento di Scienze Chimiche, Università di Cagliari, Cittadella Universitaria di Monserrato, Strada Statale 554 bivio per Sestu, 09042 Monserrato, Cagliari, Italy, and School of Physical Sciences, University of Kent, Canterbury, CT2 7NR, UK

Extended X-ray absorption fine structure and X-ray absorption near edge structure techniques were used to study in detail the formation of FeCo alloy nanoparticles in a silica matrix during their sol−gel preparation. Depending on the Fe and Co precursors, different intermediate products are formed, ferrihydrite and Co_3O_4 starting from nitrate precursors and cobalt ferrite starting from acetate precursors. The final nanocomposites contain bcc FeCo nanoparticles which are sometimes accompanied by fcc Co depending both on the intermediate products and on the porous structure of the samples.

Introduction

Materials with nanometer size particles exhibit unique chemical and physical properties.[1,2] In particular, nanocomposite materials, composed of nanometric metal and metal oxide particles embedded in vitreous matrixes, present a variety of interesting magnetic, electric, and catalytic properties that depend both on the composition of the nanophase and on the particle size.[3−6]

No much work has been done so far on nanocomposites containing alloy nanoparticles probably because of the difficulties in their stabilization with comparison to single metal or metal oxide nanoparticles.[7] The possibility of obtaining bcc FeCo alloys in nanometric form can be of interest because the alloys in bulk form possess interesting soft magnetic properties which have been thoroughly studied over the years.[8,9] Moreover, the presence of alloy nanoparticles in a silica matrix can give interesting non linear optical properties.[10]

Recently, the sol−gel method[11] proved to be successful for the formation of aerogel and xerogel nanocomposites containing bcc FeCo nanoparticles dispersed into amorphous silica.[12,13] In the case of the aerogel samples, which are characterized by high surface area and pore volume, FeCo nanoparticles of the desired composition were obtained starting from nitrate metallic precursors,[12] whereas in order to obtain the alloy of the desired composition, acetate precursors had to be used for xerogel samples, which are denser materials with respect to the aerogel samples.[13] The structural characterization of the samples, which was performed by X-ray diffraction, did not completely clarify the nature of the intermediate products formed during the different stages of the preparation which should help understanding the different behavior among the different samples. This was mostly due to the low concentration of the nanocrystalline phase with respect to the silica matrix and to the difficulty of distinguishing cobalt and iron which have very similar X-ray scattering factors.

In this paper, X-ray absorption spectroscopy techniques have been used to examine FeCo−SiO2 nanocomposites in order to gain selective and detailed information on the evolution of the precursors during the sol−gel preparation of aerogels, xerogels, and films.

X-ray absorption techniques are very suitable methods because they are elemental specific and, hence, can examine the Fe and Co atom environment separately and can give valuable information even in the case of dilute samples.[14] The use of these techniques has already proved to give valuable information for the study of nanocomposites prepared by sol−gel.[15,16] Quantitative structural information about the metal atom environment in complex materials can be obtained from extended X-ray absorption fine structure (EXAFS) spectra in terms of number and type of neighboring atoms around a selected absorbing atom, interatomic distances, and Debye−Waller factors. X-ray absorption near edge structure (XANES) can also provide information about the metal atom environment.

Experimental Section

Sample Preparation. FeCo−SiO2 nanocomposites in the form of xerogels, aerogels, and films were prepared by the sol−gel method: more details can be found in refs 12 and 13. Tetraethoxysilane (TEOS, Aldrich 98%) was used as precursor for the SiO2, whereas either metal nitrates ($Fe(NO_3)_3\cdot9H_2O$, Aldrich 98% and $Co(NO_3)_2\cdot6H_2O$, Aldrich 98%) or metal acetates ($Fe(CH_3CO_2)_2$, Aldrich 95% and $Co(CH_3CO_2)_2\cdot4H_2O$, Aldrich 98%) were used as precursors for the FeCo nanoparticles. In the first case, the nitrate salts were dissolved in ethanol (EtOH, Carlo Erba 95%) and then added to a solution of TEOS in ethanol, a few drops of HNO3 (Carlo Erba 70%) were also added in order to keep the pH between 0.6 and 0.8; the hydrolysis was promoted only by the water present in the EtOH and in the salts as crystallization water. When using the acetates, water was added to promote the dissolution of the salts and acetic acid was used as catalyst. The starting solution was kept under vigorous stirring for 1 h and then poured into Teflon beakers. The sol was then allowed to gel in air at room temperature. The xerogel samples were obtained by treating the

* To whom correspondence should be addressed. Phone: +39 070 6754351. Fax: +39 070 6754388. E-mail: corrias@unica.it.
† Università di Cagliari.
‡ University of Kent.

gel in air at 350 °C for 1 h and the final samples were obtained by a further treatment in hydrogen flow at 800 °C for 2 h. A xerogel film sample was obtained by dip-coating, i.e., by first dipping a quartz substrate in the sol aged for 3 days and then pulling the substrate at constant speed (3.3 mm s⁻¹) using a motor driven apparatus. After the first dip, the film was dried at 50 °C in air and then submitted to further two dipping in order to achieve a thickness around 100 nm. The deposited films were submitted to the same thermal treatment as the xerogel samples using a tubular quartz reactor with a rotating sample holder in order to ensure homogeneous heating conditions. In the case of the aerogels, the solvent was removed from the wet gel by high-temperature supercritical drying in an autoclave. Two different conditions of supercritical drying were used, which differ in the heating ramp, the initial pressure and the solvent used to fill the autoclave. It has been shown that these conditions are able to produce either mesoporous or microporous aerogels.[12,17−19] After supercritical drying, the aerogels were submitted to the same treatments as the xerogels, i.e., at 350 °C in air for 1 h and at 800 °C in hydrogen flow for 2 h.

Data Collection. The X-ray absorption spectroscopy experiments were carried out on station 8.1 of the SRS, Daresbury Laboratory, U.K. Data were collected at the Fe and Co K edges on two xerogel samples, one obtained from acetate precursors (X-Ac) and one from nitrate precursors (X-Nit), on two aerogel samples obtained using the nitrate precursors, one mainly mesoporous (A1-Nit) and the other one mainly microporous (A2-Nit), and on one film obtained from acetate precursors (F−Ac). Data were collected both on the samples treated at 350 °C in air and after the final treatment at 800 °C in hydrogen flow. Data were also collected on some reference compounds: commercial 2-line ferrihydrite (Aldrich 98%) and Co₃O₄ (Aldrich 99%), cobalt ferrite (CoFe₂O₄) prepared following the method reported by Lee et al.,[20] and bcc Fe and fcc Co foils. The X-ray absorption spectra were collected in transmission mode at room temperature for all of the samples apart from the film samples whose data were collected in fluorescence mode. Samples with high uniformity and a suitable optical thickness were prepared from powders which were dispersed in an inert solvent and then filtrated onto polythene supports, whereas the films were measured without any further treatment. Ion chambers before and after the samples were used to measure the incident and transmitted intensities, I_0 and I_t, respectively, whereas the intensity of fluorescence signal, I_f, emitted from the sample was measured using a solid-state detector.

A double Si(111) monochromator was used; higher order harmonic rejection was achieved by detuning the monochromator so that the transmitted flux was reduced by 50%. In the EXAFS region, absorption was measured at constant k intervals. In the XANES region, spectra were collected with intervals of approximately 0.25 eV. The resolution of the monochromator is approximately 1 eV in the energy range studied. The energies of the first inflection point for Fe and Co foils was taken to be 7112 and 7709 eV, respectively.[21] The energy scale was calibrated by simultaneously measuring the absorption through a 5 μm thick Fe or Co foils, by using a third ion chamber. The energies of XANES features were detectable to an accuracy of 0.5 eV.

EXAFS Data Analysis. Data analysis was carried out using the suite of programs at the Daresbury Laboratory.[22] EXCALIB was used to normalize the transmitted (or the fluorescence) X-ray intensity, I_t, to the incident X-ray intensity, I_0, and hence to obtain absorbance $\mu t = \ln(I_0/I_t)$. EXBACK was used to identify the beginning of the absorption edge, E_0, to fit preedge

and postedge backgrounds, μt_{pre} and μt_{post} respectively, and hence to obtain the normalized absorbance $\chi = (\mu t - \mu t_{post})/(\mu t_{post} - \mu t_{pre})$.

The final stage of data processing was to extract structural information by using EXCURV98 to model the experimental $\chi(k)$ using fast curved wave theory[23] where

$$\chi(k) = \sum_i S_0^2(k)\,(N_i/kR_i^2)\,|f_i(k,R)|\,\sin(2kR_i + 2\delta(k) + \varphi_i(k,R))\,\exp(-2\sigma_i^2 k^2)\,\exp(-2R_i/\lambda(k)) \quad (1)$$

and k is the modulus of the wave-vector of the photoelectron, R_i, N_i, and $2\sigma_i^2$ are the distance, coordination number, and Debye−Waller term (because of static and thermal disorder) for the ith shell of neighboring atoms. The additional parameters in eq 1 are the effective curved wave backscattering amplitude $f(k,R)$ of the scatterer, the phase shift due to the absorbing atom potential $2\delta(k)$, the phase shift due to the scatterer $\varphi_i(k,R)$, and the inelastic mean free path of the photoelectron $\lambda(k)$.

Equation 1 is valid for single scattering of the photoelectron. However, multiple scattering can be significant depending on the structure.[23] fcc and bcc lattices are examples of compounds where multiple scattering is expected to be particularly strong for certain shells because of a forward-scattering path (also called the focusing or shadowing effect) consisting of collinear arrangements of neighboring atoms.[24] In EXCURV98, the effect of multiple scattering can be included either by calculating all of the multiple scattering paths within clusters centred on the central atom or by adding only the contribution of the most significant multiple scattering paths by defining the atoms involved, as discussed later.

The fitting was carried out in k space in the range 2.5−12.5 Å⁻¹; at the Fe edge 12.5 Å⁻¹ is the upper accessible k value because of the presence of the Co K edge; the same k range was used at the Co edge to achieve a similar resolution. Theoretical parameters $|f_i(k,R_i)|$, $\varphi_i(k,R_i)$, $\delta(k)$, and $\lambda(k)$ were calculated using the von Barth potential for ground states, the Hedin−Lundquist exchange potential for excited states,[25] and the relaxed approximation for the core-hole.[26] In EXCURV98 the k-independent parameter AFAC takes the place of $S_0(k)^2$ in eq 1. AFAC was determined to be 0.9 from fitting to the reference samples. The parameter EF, which is a correction to E_0, was free to vary in all fitting.

The structural parameters were obtained by nonlinear least-squares fitting in k-space with a k³ weighting of the total experimental EXAFS spectra. The quality of the fit can be judged from the normalized sum of residuals

$$R\ \text{factor} = \Sigma_n\,|k_n^3\chi_{expt}(k_n) - k_n^3\chi_{fit}(k_n)|/$$
$$\Sigma_n\,|k_n^3\chi_{expt}(k_n)| \times 100 \quad (2)$$

Although reasonable EXAFS fits of single shells typically have values around 20%, when the fit is performed on the total EXFAS spectra, higher values can still correspond to good fits especially if the fit is not extended to peaks at high R. For this reason, the R factors were calculated both on the experimental $k^3\chi(k)$ and on the data obtained by inverse transforming the Fourier transform in the range corresponding to the shells which were actually fitted. The errors in the fit parameters R_i, N_i, and $2\sigma_i^2$ were obtained from the 95% confidence level as calculated in EXCURV98.

XANES Data Analysis. The XANES spectra were processed in the usual way to obtain normalized absorbance.[27] XANES at the K edge involves the excitation of a 1s photoelectron into low-lying empty states at the central atom with p-type symmetry.
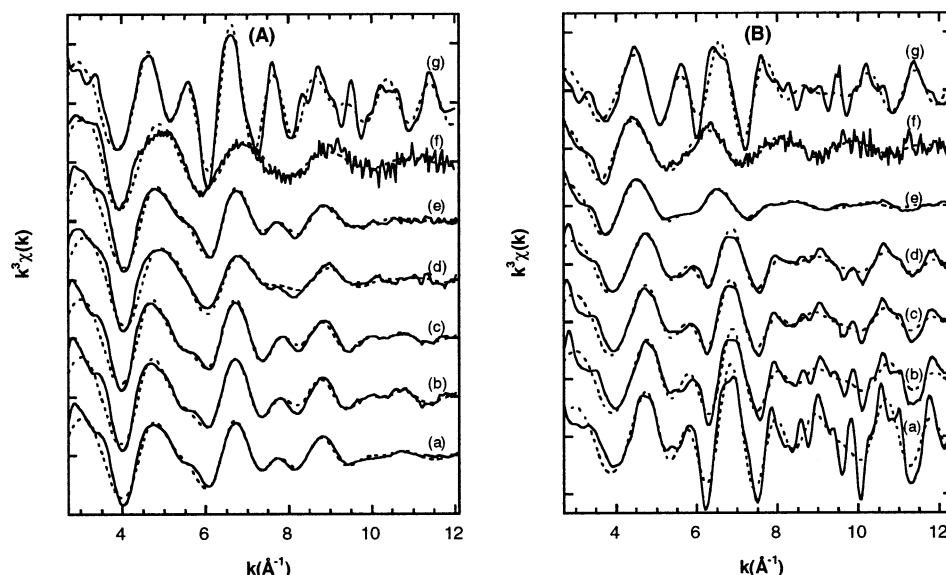
Figure 1. $k^3\chi(k)$ spectra from experiment (—) and fit results (···) for the samples treated at 350 °C and for the reference compounds. (A) Fe K edge: (a) ferrihydrite, (b) A1-Nit, (c) A2-Nit, (d) X-Nit, (e) X-Ac, (f) F-Ac, (g) $CoFe_2O_4$. (B) Co K edge: (a) Co_3O_4, (b) A1-Nit, (c) A2-Nit, (d) X-Nit, (e) X-Ac, (f) F-Ac, (g) $CoFe_2O_4$.

The characteristic features of the XANES spectra for transition metal oxides[21] are as follows. An increase in valence of the metal atom causes a shift to higher energies. Preedge peak(s) may occur corresponding to 1s to 3d transitions with 3d−4p mixing. The preedge peak increases in intensity as the degree of centrosymmetry of the metal atom environment decreases. The main peak and shoulders of the absorption edge corresponds to transitions to 4p continuum states and "shape resonances" of the metal atom environment. For a given environment, the main peak is broadened by disorder in the nearest neighbor distances. Secondary peaks occurring a few 10 eV above the main peak correspond to multiple scattering from neighboring atom shells.

Results

Samples Treated at 350 °C in Air. In Figure 1A, the EXAFS spectra at the Fe K edge for the samples treated at 350 °C are compared with those of 2-line ferrihydrite and $CoFe_2O_4$. The spectrum of $CoFe_2O_4$ shows oscillations up to high k as expected for a crystalline compound. On the other hand, the spectrum of ferrihydrite shows much smaller oscillations; this can be ascribed to the structure of ferrihydrite, a poorly crystalline Fe(III) oxyhydroxide whose XRD spectrum shows from two to six broad diffraction lines (2-line and 6-line ferrihydrite, respectively).[28] Despite the difference in the amplitude of the oscillations between $CoFe_2O_4$ and ferrihydrite the frequencies seem to be quite similar. The spectra of all of the xerogel and aerogel samples look similar in frequencies and amplitude to the one of ferrihydrite. The spectrum of sample F−Ac collected in fluorescence mode is much noisier compared with the ones collected in transmission mode and seems dominated by a single shell contribution.

In Figure 1B, the EXAFS spectra at the Co K edge for the same samples are compared with those of Co_3O_4 and $CoFe_2O_4$. The spectra of both reference compounds show strong oscillations up to high k as expected for crystalline compounds. The spectra of the samples obtained starting from nitrate precursors, i.e., A1-Nit, A2-Nit, and X-Nit, show very similar oscillations to those of Co_3O_4 with slightly reduced amplitude while the spectrum of sample X-Ac is definitely different and seems more

similar to $CoFe_2O_4$ even if the oscillations are strongly reduced in amplitude. The spectrum of sample F−Ac is again much noisier than the spectra of the other samples but nevertheless seems to bear a stronger resemblance to the one of sample X-Ac.

These results are also confirmed by the modulus of the Fourier transform (FT) at the Fe and Co K edge for the same samples, which are reported in Figure 2, parts A and B. The FTs of $CoFe_2O_4$ at both edges show evident peaks up to high R values as well as the FT of the Co_3O_4 sample, whereas the FT of ferrihydrite only shows a small peak beyond the first shell as a consequence of its poor crystallinity. The FTs of all of the samples at the iron edge are quite similar to ferrihydrite. The FTs of the samples at the Co edge confirm that the samples obtained from nitrate contain Co_3O_4 with higher disorder and/or smaller crystallite size compared to the reference compound because all of the shells are broader. The broadening is even more pronounced in the samples obtained from acetate precursors, whose FTs seem more similar to $CoFe_2O_4$.

In Figure 3, parts A and B, the measured XANES at the Fe and Co K edge, respectively, are shown for the samples treated at 350 °C in air and for the reference compounds. The Fe edge XANES spectra for samples A1-Nit and A2-Nit are very similar to ferrihydrite. The Fe edge for sample X-Nit is similar, but there is noticeable broadening of features which is consistent with greater disorder or reduced crystalline size. The Fe edge for sample X-Ac shows a small multiple scattering peak at 28 eV and considering this seems more similar to the Fe edge for $CoFe_2O_4$ but with less pronounced peaks at 21, 28, and 35 eV. The Fe edge for sample F-Ac is difficult to compare due to greater noise.

The Co edge XANES spectra for sample A1-Nit and A2-Nit have shapes very similar to Co_3O_4 which is most obvious in the region of 15−35 eV. The Co edge for sample X-Nit is similar, but with a less well-defined main absorption edge peak which is consistent with greater disorder or reduced crystalline size. On the other hand, the Co edge XANES spectra for samples X-Ac and F-Ac have broader absorption edge peaks which seem more similar to $CoFe_2O_4$. These observations are consistent with those from EXAFS.

The qualitative comparison of the experimental EXAFS and XANES spectra at both the iron and cobalt edge with those of
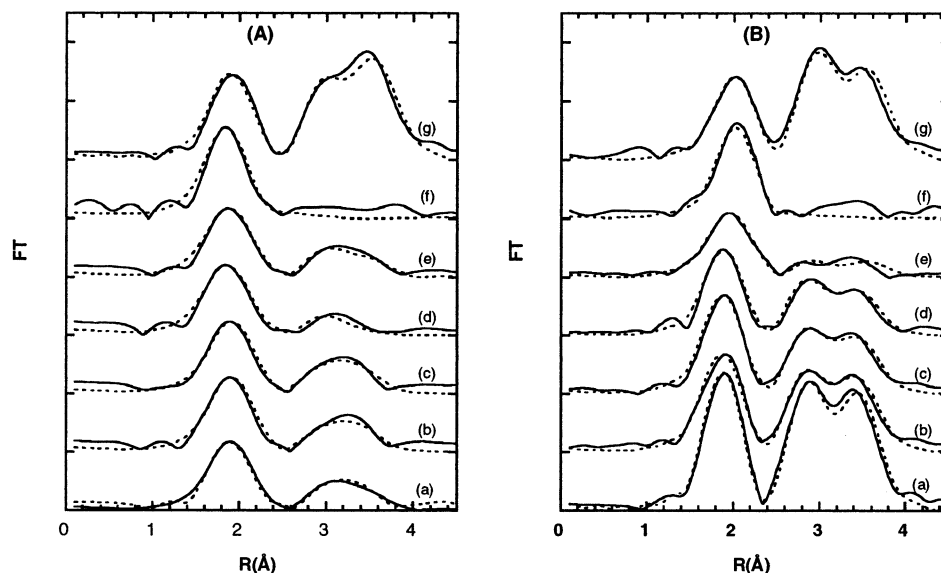
Figure 2. Modulus of Fourier transforms of $k^3\chi(k)$ spectra from experiment (—) and fit results (···) for the samples treated at 350 °C and for the reference compounds. (A) Fe K edge: (a) ferrihydrite, (b) A1-Nit, (c) A2-Nit, (d) X-Nit, (e) X-Ac, (f) F-Ac, (g) CoFe₂O₄. (B) Co K edge: (a) Co₃O₄, (b) A1-Nit, (c) A2-Nit, (d) X-Nit, (e) X-Ac, (f) F-Ac, (g) CoFe₂O₄.
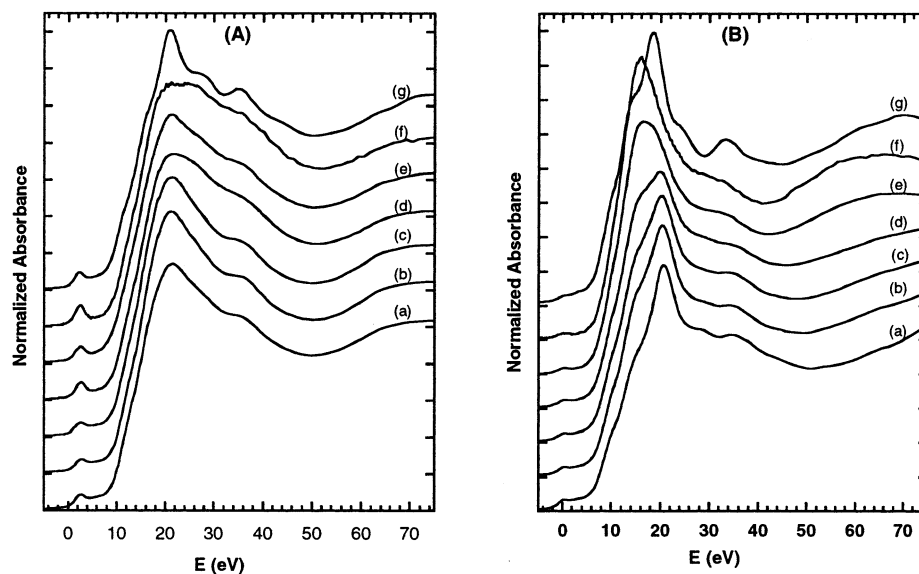
Figure 3. XANES spectra from experiment for the samples treated at 350 °C and for the reference compounds. (A) Fe K edge: (a) ferrihydrite, (b) A1-Nit, (c) A2-Nit, (d) X-Nit, (e) X-Ac, (f) F-Ac, (g) CoFe₂O₄. (B) Co K edge: (a) Co₃O₄, (b) A1-Nit, (c) A2-Nit, (d) X-Nit, (e) X-Ac, (f) F-Ac, (g) CoFe₂O₄.

the reference compounds gives some important information on the phases which are formed after calcinations of the samples at 350 °C; in particular, they indicate that the samples obtained starting from nitrate precursors contain both Co₃O₄ and ferrihydrite nanoparticles, whereas a cobalt ferrite phase should be present in the samples obtained starting from acetate precursors.

These qualitative indications were used as a basis for fitting the total EXAFS spectra. The data of the reference compounds were first used to check that the theoretical backscattering and phase shifts calculated by EXCURV98 were acceptable. According to literature, the structure of CoFe₂O₄ is a partially inverse spinel with 80% of Co²⁺ in tetrahedral sites and 20% in octahedral sites and 60% of Fe³⁺ in tetrahedral sites and 40% in octahedral sites.[29] This means that the environment around Fe³⁺ and Co²⁺ has shells with the same R_i but with different N_i as a consequence of the different occupation of the sites. The first FT peak, centered around 2 Å at both edges, was fitted with a single O shell coming from both the tetrahedral and

octahedral sites, whereas the further peaks up to 4 Å were fitted with 2 shells of metal—metal contributions. Because Fe and Co have very similar backscattering amplitudes in order to simplify the fitting only Fe backscatterers were considered at the Fe edge and only Co backscatterers at the Co edge. The fit was carried out keeping N_i fixed to those of the known crystal structure, allowing small variations of the R_i values within the experimental error, whereas the $2\sigma_i^2$ parameters were free to vary together with EF. The Co₃O₄ structure is a direct spinel,[30] i.e., with Co²⁺ in tetrahedral sites and Co³⁺ in octahedral sites. Also in this case, the first FT peak was fitted with a single O shell coming from both the tetrahedral and octahedral sites, whereas the further peaks up to 4 Å were fitted with 2 shells of Co—Co contributions. In the case of the ferrihydrite sample, whose structure is not so well established because of its poor crystallinity, the starting R_i and N_i parameters were chosen in accordance with the data available in the literature,[28] but they were left free to vary together with $2\sigma_i^2$ and EF.

TABLE 1: Interatomic Distances (R), Coordination Numbers (N), and Debye−Waller Factors (σ) Obtained by Fitting the Experimental EXAFS Spectra of the Reference Compounds at the Fe and Co Edge[a]

| | Fe edge | | | | | | atom | Co edge | | | | | |
| | Ferrihydrite | | | CoFe$_2$O$_4$ | | | | CoFe$_2$O$_4$ | | | Co$_3$O$_4$ | | |
atom	R(Å)	N	$2\sigma^2$	R(Å)	N	$2\sigma^2$	atom	R(Å)	N	$2\sigma^2$	R(Å)	N	$2\sigma^2$
O	1.95 (1)	5.1 (2)	0.021 (2)	1.95 (1)	*5.2*	0.020 (3)	O	2.05 (1)	*5.6*	0.018 (3)	1.92 (1)	*5.3*	0.009 (2)
Fe	2.87 (3)	0.8 (3)	0.019 (6)	2.97 (1)	*3.6*	0.013 (2)	Co	2.97 (1)	*4.9*	0.013 (2)	2.86 (1)	*4.0*	0.008 (1)
Fe	3.02 (1)	2.4 (4)	0.020 (3)	3.49 (1)	*8.4*	0.016 (1)	Co	3.49 (1)	*7.15*	0.016 (2)	3.37 (1)	*8.0*	0.014 (2)
Fe	3.42 (3)	1.5 (6)	0.020 (6)										
	R factor = 26%			R factor = 37%				R factor = 46%			R factor = 48%		
	*R factor = 16%			*R factor = 19%				*R factor = 26%			*R factor = 23%		

[a] Parameters taken from the literature are indicated in italic. Errors shown in brackets for the parameters free to vary during fitting. R factors calculated on the original data, *R factors calculated on the backtransforms as described in the text.

TABLE 2: Interatomic Distances (R), Coordination Numbers (N), and Debye−Waller Factors (σ) Obtained by Fitting the Experimental EXAFS Spectra of the Samples Treated at 350 °C at the Fe Edge[a]

| | A1-Nit | | | A2-Nit | | | X-Nit | | | X-Ac | | | F−Ac | | |
atom	R(Å)	N	$2\sigma^2$	R(Å)	N	$2\sigma^2$	R(Å)	N	$2\sigma^2$	R(Å)	N	$2\sigma^2$	R(Å)	N	$2\sigma^2$
O	1.97 (1)	5.8 (3)	0.022 (2)	1.97 (1)	5.7 (3)	0.023 (2)	1.92 (1)	5.7 (2)	0.025 (2)	1.94 (1)	5.2 (2)	0.024 (2)	1.90 (1)	5.2 (3)	0.021 (2)
Fe	2.87 (2)	1.4 (4)	0.018 (5)	2.87 (2)	1.4 (4)	0.018 (5)	2.97 (2)	2.3 (6)	0.027 (5)	2.99 (1)	2.7 (5)	0.027 (4)			
Fe	3.03 (1)	2.4 (4)	0.018 (3)	3.02 (1)	2.4 (4)	0.018 (3)				3.48 (3)	1.7 (7)	0.025 (7)			
Fe	3.41 (3)	1.4 (6)	0.017 (5)	3.41 (3)	1.4 (6)	0.017 (6)									
	R factor = 29%			R factor = 29%			R factor = 28%			R factor = 30%			R factor = 37%		
	*R factor = 16%			*R factor = 13%			*R factor = 24%			*R factor = 21%			*R factor = 26%		

[a] Errors shown in brackets for the parameters free to vary during fitting. R factors calculated on the original data, *R factors calculated on the backtransforms as described in the text.

The results of the fitting of the reference compounds are shown in Figures 1 and 2, and the best fitting parameters are reported in Table 1. The R factors calculated backtransforming the FTs in the range actually used in the fit are quite good confirming that the calculated phase shifts and amplitudes can be used to fit the data of the samples. It can be noticed that the fit quality of the CoFe$_2$O$_4$ spectrum at the Fe edge is better than the one at the Co edge. Moreover, the difference between R_{Co-O} and R_{Fe-O} is larger than expected on the basis of the percentage of Co ions in octahedral sites with respect to Fe. This might be due to a different distribution of the Co and Fe ions into the tetrahedral and octahedral sites with respect to the data reported in the literature for the known crystal structure.

The fits of the samples were done using the indications given from the comparison of their experimental data with those of the reference compounds. Some of the samples show a reduced amplitude of the EXAFS oscillations compared with the reference samples. This can be due either to an increase of the Debye−Waller factors or to a reduction of the coordination number of the outer shells because of the large fraction of atoms near the surface of the nanoparticles. It is not straightforward to discriminate between the two possibilities in a multishell fitting, because N_i and $2\sigma_i^2$ are strongly correlated. It should be pointed out that a significant reduction of the coordination number for outer shells is expected to occur for particles smaller than 5−6 nm.[31] Because TEM observations giving the average particles size are available (the average particle size decreases from 5 to 3 nm going from sample A1-Nit, A2-Nit, X-Nit, and X-Ac samples),[12,13] these were taken into account during the fitting.

The results of the fitting at the Fe edge for the samples treated at 350 °C are shown in Figures 1A and 2A and the best fitting parameters are reported in Table 2. Because of the close resemblance of the experimental spectra of samples A1-Nit and A2-Nit with that of ferrihydrite, the same number of shells, i.e., one shell of O and three shells of Fe, were used in the fitting, whereas for sample X-Nit, which is less structured, only one shell of O and 1 shell of Fe were used. In the case of sample X-Ac, the same shells as in CoFe$_2$O$_4$ were used, i.e., one shell of O and two shells of Fe, whereas in the case of sample F−Ac, only one shell of O was used. The fits are quite good for all of the samples and confirm the presence of Fe(III) oxyhydroxide nanoparticles in samples A1-Nit and A2-Nit with similar particle size and disorder as in ferrihydrite because similar R_i, N_i, and $2\sigma_i^2$ were obtained. In the case of sample X-Nit, the results are compatible with the presence of Fe(III) oxyhydroxide nanoparticles with significantly smaller particle size and higher disorder than in ferrihydrite because the coordination number for the 2nd shell is lower with respect to the ferrihydrite and has a higher $2\sigma^2$. In the case of sample X-Ac, the results of the fitting indicate the presence of small nanoparticles of cobalt ferrite because the coordination number of the 2nd and 3rd shell are significantly smaller than CoFe$_2$O$_4$. The nanoparticles are probably even smaller in sample F-Ac, which was fitted with a single O shell, even if some higher shell contribution might not be detectable due to the higher noise.

The results of the fitting at the Co edge for the same samples are shown in Figures 1B and 2B, and the best fitting parameters are reported in Table 3. In this case, all of the samples obtained starting from nitrate precursors were fitted using the same shells as in Co$_3$O$_4$ and X-Ac using the same shells as in CoFe$_2$O$_4$, i.e., in both cases one O and two Co shells, whereas sample F-Ac was fitted with a single O shell. The fits are reasonably good and confirm the presence of Co$_3$O$_4$ in the samples obtained from nitrate precursors. The N_i are about the same as in Co$_3$O$_4$ in sample A1-Nit, whereas the ones for the 2nd and 3rd shells become smaller in A2-Nit and even smaller in X-Nit indicating the presence of smaller nanoparticles in the last two samples; the disorder in the nanoparticles is always higher than in the reference compound. The N_i of the 2nd and 3rd shells for sample X-Ac are smaller than those of CoFe$_2$O$_4$ at the same extent as at the Fe edge confirming the presence of small cobalt ferrite nanoparticles. As already mentioned, sample F-Ac, which was fitted with a single O shell contribution, might have smaller cobalt ferrite nanoparticles than sample X-Ac but the presence of higher shell contribution cannot be ruled out due to the noise.

Spectroscopy Study of FeCo–SiO₂ Nanocomposites

J. Phys. Chem. B, Vol. 107, No. 13, 2003 **3035**

TABLE 3: Interatomic Distances (R), Coordination Numbers (N), and Debye–Waller Factors (σ) Obtained by Fitting the Experimental EXAFS Spectra of the Samples Treated at 350 °C at the Co Edge[a]

	A1-Nit			A2-Nit			X-Nit			X-Ac			F-Ac		
atom	R(Å)	N	$2\sigma^2$	R(Å)	N	$2\sigma^2$	R(Å)	N	$2\sigma^2$	R(Å)	N	$2\sigma^2$	R(Å)	N	$2\sigma^2$
O	1.91 (1)	5.3 (4)	0.016 (2)	1.92 (1)	5.3 (3)	0.016 (2)	1.93 (1)	4.5 (2)	0.015 (2)	2.01 (1)	5.5 (2)	0.025 (2)	2.06 (1)	5.5 (3)	0.015 (2)
Co	2.84 (1)	3.9 (5)	0.016 (2)	2.86 (1)	3.2 (4)	0.016 (2)	2.85 (1)	2.7 (4)	0.016 (2)	2.95 (3)	1.6 (5)	0.030 (8)			
Co	3.35 (1)	7.8 (9)	0.022 (2)	3.37 (1)	5.6 (8)	0.022 (2)	3.37 (1)	4.5 (7)	0.022 (2)	3.49 (2)	2.6 (8)	0.030 (8)			
	R factor = 43%			R factor = 36%			R factor = 35%			R factor = 27%			R factor = 42%		
	*R factor = 27%			*R factor = 26%			*R factor = 23%			*R factor = 20%			*R factor = 26%		

[a] Errors shown in brackets for the parameters free to vary during fitting. R factors calculated on the original data, *R factors calculated on the backtransforms as described in the text.
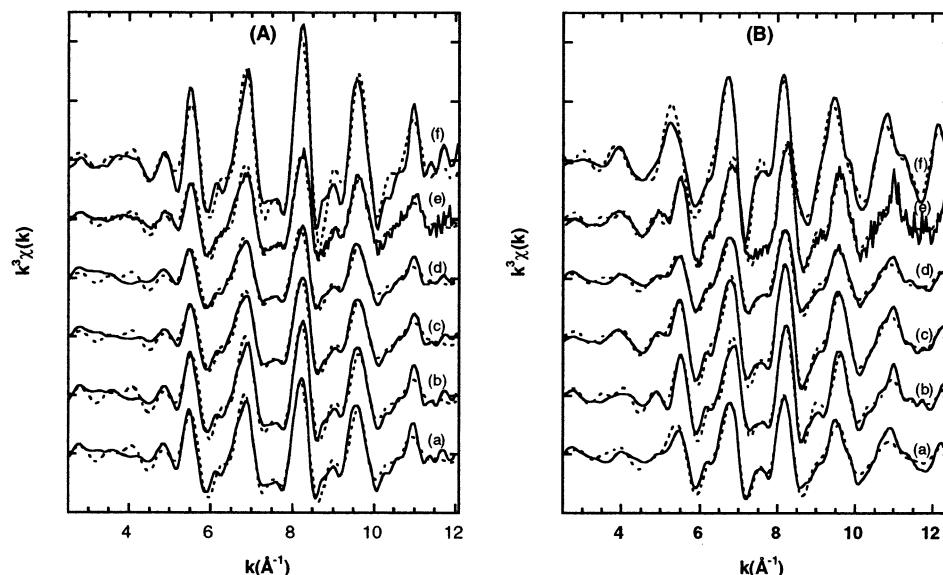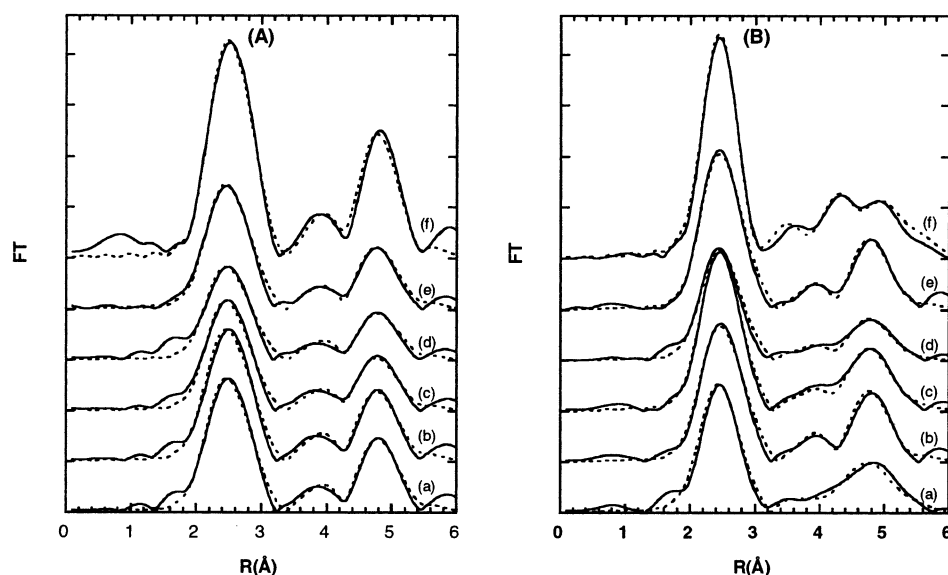

Figure 4. $k^3\chi(k)$ spectra from experiment (—) and fit results (⋯) for the samples treated at 800 °C and for the reference compounds. (A) Fe K edge: (a) A1-Nit, (b) A2-Nit, (c) X-Nit, (d) X-Ac, (e) F-Ac, (f) bcc Fe. (B) Co K edge: (a) A1-Nit, (b) A2-Nit, (c), X-Nit (d) X-Ac, (e) F-Ac, (f) fcc Co.

Samples Reduced at 800 °C in H₂ Flow. In Figure 4, parts A and B, the EXAFS spectra at the Fe and Co K edge respectively are reported for the samples treated at 800 °C in H₂ flow. At the Fe edge, the spectra are compared with that of bcc Fe and at the Co edge with that of fcc Co. All of the spectra of the samples at the Fe edge are quite similar to that of bcc Fe apart from a reduction in the amplitude of the oscillations indicating a similar Fe environment. On the other hand, the spectra of the samples at the Co edge are actually more similar to bcc Fe than to fcc Co which is expected if a bcc FeCo alloy is formed. This is also confirmed by the corresponding FTs, which are reported in Figure 5, parts A and B, for the Fe and Co edge, respectively. Some differences can be noticed among the different samples. Samples A2-Nit and F-Ac are the ones whose spectra at both edges look more alike and similar to bcc Fe. In sample A1-Nit, the presence of some fcc Co together with the bcc phase can be noticed as well as in sample X-Nit and probably in sample X-Ac, whose data are the ones which show the highest reduction in the amplitude of the oscillations and a corresponding largest peak broadening in the FTs.

In Figure 6, parts A and B, the measured XANES at the Fe and Co K edge, respectively, are shown for the samples treated at 800 °C. All of the samples show XANES spectra more similar to bcc sample with main absorption edge peak at 20 eV and no spread from 15 to 25 eV as for the fcc sample. The bcc spectrum is also characterized by a multiple scattering peak at 30 eV which is most visible in the Fe edge of samples A1-Nit and A2-Nit and Co edge of samples A2-Nit and F-Ac. This is consistent with almost complete bcc environment in these

samples. The Fe edges of samples X-Nit and X-Ac show reduction of the bcc multiple scattering peak and a broad negative gradient over the range 20–50 eV which is consistent with a significant contribution from oxide phase (see Figure 5A). Similarly, the Co edges of samples A1-Nit and X-Ac show reduction of the bcc multiple scattering peak which is consistent with a significant proportion of Co not being in bcc phase. These observations are consistent with those from EXAFS.

The qualitative comparison of the EXAFS and XANES data of the samples with those of bcc Fe and fcc Co was taken as a basis for the fitting procedures. First of all the data of the bcc Fe and fcc Co were used to test the calculated phase shift and amplitudes. For bcc Fe, the first 6 shells of the known crystalline structure were taken.[32] The first two shells correspond to the first FT peak, the 3rd shell correspond to the second FT peak and the 4th, 5th, and 6th shell to the third FT peak. In the case of the bcc Co sample, the first 5 shells of the known crystalline structure were taken into account.[33] The first shell corresponds to the first FT peak, the further ones correspond to the not well resolved peaks between 3 and 6 Å. The multiple scattering path involving the collinear arrangement of the Fe atoms in the 1st and 5th shell of the bcc structure and of the Co atoms in the 1st and 4th shell of the fcc structure were also taken into account since their contribution is quite large.[24] The Rehr and Albers approximation was used to calculate the multiple scattering contributions.[33,34] The N_i values were kept fixed during the fitting and the distances of the shells beyond the first one were kept equal to the expected R_i/R_1 ratios. Small variation of R_1 were allowed, and $2\sigma_i^2$ and EF were free to vary during fitting.

Figure 5. Modulus of Fourier transforms of $k^3\chi(k)$ spectra from experiment (—) and fit results (···) for the samples treated at 800 °C and for the reference compounds. (A) Fe K edge: (a) A1-Nit, (b) A2-Nit, (c) X-Nit, (d) X-Ac, (e) F-Ac, (f) bcc Fe. (B) Co K edge: (a) A1-Nit, (b) A2-Nit, (c), X-Nit (d) X-Ac, (e) F-Ac, (f) fcc Co.
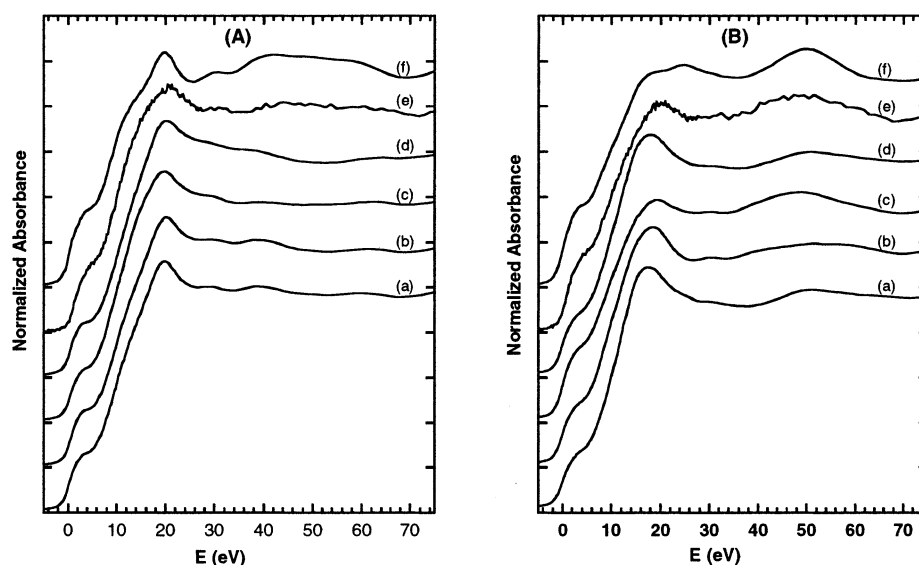
Figure 6. XANES spectra from experiment for the samples treated at 800 °C and for the reference compounds. (A) Fe K edge: (a) A1-Nit, (b) A2-Nit, (c) X-Nit, (d) X-Ac, (e) F-Ac, (f) bcc Fe. (B) Co K edge: (a) A1-Nit, (b) A2-Nit, (c), X-Nit (d) X-Ac, (e) F-Ac, (f) fcc Co.

In both cases, the result of the fit is good and confirm that the calculated phase shifts and backscattering amplitudes can be used for fitting the data of the samples.

The data of the samples treated at 800 °C at the Fe edge were fitted using the same number of shells as in the bcc Fe. The experimental data show a reduced amplitude of the EXAFS oscillations compared with the reference sample. This was attributed mainly to an increase of the $2\sigma_i^2$ because TEM observations indicated that in all of the samples the average particle size is between 9 and 10 nm.[12,13] Therefore, the N_i/N_1 ratios were kept consistent with a bcc structure as well as the R_i/R_1 ratios.

The results of the fitting are shown in Figure 4A and 5A, and the best fitting parameters are reported in Table 5. The results indicate that in all cases the Fe environment is the typical one of a bcc structure with distances very close with those of bcc Fe and larger $2\sigma_i^2$. The coordination numbers of samples A1-Nit and A2-Nit are exactly the same as in bcc Fe, and there is a 10% decrease of the N_i of F-Ac sample and reductions of

TABLE 4: Interatomic Distances (R), Coordination Numbers (N), and Debye–Waller Factors (σ) Obtained by Fitting the Experimental EXAFS Spectra of the bcc Fe and fcc Co Reference Compounds[a]

	bcc Fe				fcc Co		
atom	R(Å)	N	$2\sigma^2$	atom	R(Å)	N	$2\sigma^2$
Fe	2.47 (1)	*8.0*	0.010 (1)	Co	2.51 (1)	*12.0*	0.013 (1)
Fe	2.85	*6.0*	0.012 (2)	Co	3.55	*6.0*	0.018 (4)
Fe	4.03	*12.0*	0.018 (4)	Co	4.34	*24.0*	0.023 (2)
Fe	4.73	*24.0*	0.015 (2)	Co	5.02	*12.0*	0.021 (2)
Fe	4.94	*8.0*	0.014 (2)	Co	5.61	*24.0*	0.030 (9)
Fe	5.71	*6.0*	0.017 (9)				
	R factor = 37%				R factor = 26%		
	*R factor = 18%				*R factor = 20%		

[a] Parameters taken from the literature are indicated in italic. Errors shown in brackets for the parameters free to vary during fitting. *R* factors calculated on the original data, *R* factors calculated on the backtransforms as described in the text.

27.5 and 30% for the samples X-Nit and X-Ac, respectively. Even taking into account the errors in the coordination numbers,

Spectroscopy Study of FeCo–SiO₂ Nanocomposites

J. Phys. Chem. B, Vol. 107, No. 13, 2003 **3037**

TABLE 5: Interatomic Distances (R), Coordination Numbers (N), and Debye Waller Factors (σ) Obtained by Fitting the Experimental EXAFS Spectra of the Samples Reduced at 800 °C at the Fe Edge[a]

	A1-Nit			A2-Nit			X-Nit			X-Ac			F-Ac		
atom	$R(Å)$	N	$2\sigma^2$	$R(Å)$	N	$2\sigma^2$	$R(Å)$	N	$2\sigma^2$	$R(Å)$	N	$2\sigma^2$	$R(Å)$	N	$2\sigma^2$
Fe	2.48 (1)	8.0 (4)	0.017 (1)	2.47 (1)	8.0 (4)	0.018 (1)	2.47 (1)	5.8 (3)	0.015 (1)	2.48 (1)	5.6 (3)	0.017 (1)	2.47 (1)	7.2 (3)	0.016 (1)
Fe	2.86	6.0	0.023 (2)	2.85	6.0	0.022 (2)	2.85	4.3	0.022 (2)	2.86	4.2	0.024 (3)	2.85	5.4	0.023 (2)
Fe	4.04	12.0	0.025 (2)	4.03	12.0	0.025 (3)	4.03	8.6	0.024 (3)	4.04	8.4	0.026 (3)	4.03	10.8	0.027 (3)
Fe	4.74	24.0	0.023 (2)	4.73	24.0	0.024 (2)	4.73	17.3	0.023 (2)	4.74	16.8	0.024 (2)	4.73	21.6	0.024 (2)
Fe	4.95	8.0	0.022 (2)	4.94	8.0	0.023 (2)	4.94	5.8	0.023 (3)	4.95	5.6	0.024 (4)	4.94	7.2	0.024 (3)
Fe	5.72	6.0	0.026 (9)	5.70	6.0	0.026 (9)	5.70	4.3	0.025 (9)	5.72	4.2	0.027 (9)	5.70	5.4	0.026 (9)
	R factor = 32%			*R* factor = 33%			*R* factor = 31%			*R* factor = 37%			*R* factor = 30%		
	*R factor = 23%			**R* factor = 25%			**R* factor = 22%			**R* factor = 27%			**R* factor = 21%		

[a] Errors shown in brackets for the parameters free to vary during fitting. R factors calculated on the original data, *R factors calculated on the backtransforms as described in the text.

TABLE 6: Interatomic Distances (R), Coordination Numbers (N), and Debye Waller Factors (σ) Obtained by Fitting the Experimental EXAFS Spectra of the Samples Reduced at 800 °C at the Co Edge[a]

	A1-Nit			A2-Nit			X-Nit			X-Ac			F-Ac		
atom	$R(Å)$	N	$2\sigma^2$	$R(Å)$	N	$2\sigma^2$	$R(Å)$	N	$2\sigma^2$	$R(Å)$	N	$2\sigma^2$	$R(Å)$	N	$2\sigma^2$
Fe	2.48	4.8 (3)	0.017	2.47	8.0 (3)	0.018	2.47	6.4 (2)	0.015	2.48	5.0 (2)	0.017	2.47	8.0 (3)	0.016
Fe	2.86	3.6	0.023	2.85	6.0	0.022	2.85	4.8	0.022	2.86	3.8	0.024	2.85	6.0	0.023
Fe	4.04	7.2	0.025	4.03	12.0	0.025	4.03	9.6	0.024	4.04	7.5	0.026	4.03	12.0	0.027
Fe	4.74	14.4	0.023	4.72	24.0	0.024	4.73	19.2	0.023	4.74	15.0	0.024	4.72	24.0	0.024
Fe	4.95	4.8	0.026	4.93	8.0	0.023	4.94	6.4	0.023	4.95	5.0	0.024	4.93	8.0	0.024
Fe	5.72	3.6	0.026	5.69	6.0	0.026	5.71	4.8	0.025	5.72	3.8	0.027	5.69	6.0	0.026
Co	2.49 (1)	4.5 (4)	0.023 (1)				2.49 (1)	2.4 (3)	0.016 (1)	2.49 (1)	1.4 (2)	0.013 (1)			
Co	3.52	2.2	0.024 (9)				3.52	1.2	0.023 (9)	3.52	0.7	0.019 (9)			
Co	4.32	8.9	0.025 (4)				4.32	4.8	0.024 (6)	4.31	2.8	0.026 (5)			
Co	4.98	4.5	0.026 (3)				4.98	2.4	0.025 (6)	4.98	1.4	0.027 (8)			
Co	5.57	8.9	0.028 (9)				5.57	4.8	0.026 (9)	5.57	2.8	0.030 (9)			
	R factor = 32%			*R* factor = 28%			*R* factor = 23%			*R* factor = 25%			*R* factor = 31%		
	*R factor = 27%			**R* factor = 20%			**R* factor = 17%			**R* factor = 20%			**R* factor = 17%		

[a] Errors shown in brackets for the parameters free to vary during fitting. R factors calculated on the original data, *R factors calculated on the backtransforms as described in the text.

these results seem to indicate that part of the Fe in the xerogel samples is involved in another phase which does not give a strong contribution to the EXAFS spectra, likely an oxide.

The fits of the samples at the Co K edge were slightly more complicated in some cases because of the presence of both bcc and fcc structures which increases the number of free parameters. However, the results of the fits at the Fe edge were used to fix R_i, $2\sigma_i^2$, and N_i/N_1 for the bcc contribution. When necessary, an fcc contribution was added with R_i/R_1 and N_i/N_1 kept consistent with the fcc structure.

The results of the fits are shown in Figures 4B and 5B, and the best fit parameters are reported in Table 6. Samples A2-Nit and F-Ac were fitted with only the bcc contribution and no reduction of coordination numbers indicating that in these two samples only a bcc phase is present. The fit results indicate that in sample A1-Nit ∼60% of the cobalt atoms have a bcc environment and ∼38% have an fcc environment; in sample X-Nit, ∼80% of the Cobalt atoms have a bcc environment and ∼20% have an fcc environment, and in X-Ac, ∼63% of the Cobalt atoms have a bcc environment and ∼12% have an fcc environment. The latter sample is the only one where there is a significant reduction of the coordination numbers suggesting that some of the cobalt is involved in another phase, which does not give a strong contribution to the EXAFS spectra, likely an oxide.

Discussion

The selectivity of the EXAFS and XANES techniques has allowed us to obtain very detailed and independent information on the evolution of the Fe and Co environment during the sol–gel preparation of FeCo–SiO₂ nanocomposites. In the samples calcined at 350 °C, the intermediate products depend on the iron and cobalt precursors used in the sol–gel synthesis. Ferrihydrite and Co₃O₄ are formed starting from nitrate precursors. The identification of the formation of the ferrihydrite is especially important because it was not detectable by X-ray diffraction,[12,13] because of its poor crystallinity associated with low Fe concentration. The results of the fitting are also consistent with the average size of the nanoparticles obtained by previous TEM observations.[12,13] In sample A1-Nit, which is mesoporous, larger Co₃O₄ particles are formed with respect to A2-Nit, which is microporous, indicating that the dimensions of the pores play the key role in determining the dimensions of the nanoparticles. The Co₃O₄ nanoparticles are even smaller in sample X-Nit which is also microporous. In sample X-Ac, obtained from acetate precursors, cobalt ferrite forms and the nanoparticles are only a few nm in size. The EXAFS results seem to indicate that the particles are smaller in F–Ac where a single O shell was detectable, but the data are too noisy to come to any definite conclusion. It should be pointed out that the data of sample X-Ac at the Fe edge could have also been interpreted as being due to the presence of ferrihydrite as in the samples obtained from nitrate precursors; this is due to the similarity in Fe–O and Fe–Fe distances of ferrihydrite and cobalt ferrite. However, by taking into account the EXAFS and XANES results at both edges, the presence of cobalt ferrite is confirmed in sample X-Ac as already suggested by X-ray diffraction.[13] However, the Fe: Co ratio in the sample is different from that of stoichiometric CoFe₂O₄; this implies the presence of either a cobalt ferrite where some of the Fe³⁺ are substituted by Co³⁺ or the contemporary presence of some Co₃O₄. It is not possible to distinguish between these two possibilities because both situations give rise to an increase of Co³⁺. The effect of the different precursors on the formation of different intermediate compounds

can be explained on the basis of the different coordination behavior of acetate and nitrate counterions, the acetate being bidentate and able to behave as a bridging ligand.[36]

The results on the final samples obtained after the thermal treatment at 800 °C in hydrogen flow indicate that the FeCo alloy nanoparticles can be obtained both starting from nitrate and acetate precursors even if in the case of the nitrate precursors the iron and cobalt are not in the same compound before the final treatment. However, in some cases both starting from nitrate and acetate precursors, the bcc FeCo alloy nanoparticles are accompanied by some fcc Co and/or some oxide.

It seems that both the textural properties and the precursors used in the sol−gel process play a role. In the case of the nitrate precursors, an interduffusion process has to take place during the reduction treatment in order for the FeCo alloy to form. Depending on the size of the Co_3O_4 nanoparticles, which is a direct consequence of the dimensions of the pores, and of the different surface area of the samples, the aerogels having a much higher surface area than the xerogels, the interdiffusion process can be more or less effective. As a consequence, in sample A2-Nit, only the bcc FeCo alloy of the expected composition is obtained; this can be attributed to the high surface area accompanied by the small size of the Co_3O_4 nanoparticles, which make the diffusion of the hydrogen and the interdiffusion of the cobalt easier. In sample A1-Nit, the FeCo alloy is accompanied by a significant (∼38%) amount of fcc Co, most likely because the larger Co_3O_4 nanoparticles make the interdiffusion of the Co more difficult; no indications of the presence of any residual oxide was observed indicating both that the diffusion of the hydrogen can be very effective in reducing Co_3O_4 and ferrihydrite and that the FeCo alloy nanoparticles are stable against oxidation. In sample X-Nit, the amount of fcc Co (∼20%) is lower than that in sample A1-Nit, but at the same time, some of the iron is present in an oxidized form. It is likely that the diffusion of the hydrogen in the xerogel sample is more difficult so that the reduction treatment can be less effective due to the much lower surface area in comparison with the aerogels. Moreover, also the interdiffusion of the Co into the Fe is more difficult, so that, even if in sample X-Nit the Co_3O_4 nanoparticles are quite small, some Co remains unalloyed. Mössbauer spectroscopy also gives evidence of the presence of Fe still in oxidized form.[13]

In the case of the samples obtained from acetate precursors, strong differences are observed between samples X-Ac and F-Ac because in the latter sample practically all of the Fe and Co atoms are in the FeCo alloy nanoparticles (apart from a small amount of Fe which might be in an oxidized form), whereas in the X-Ac sample, a significant fraction (∼30%) of the iron is an oxidized form and the cobalt is partly in the FeCo alloy (∼63%), partly in unalloyed Co (∼12%), and partly in oxidized form. It should be pointed out that the data of the film sample treated at 800 °C even if still slightly noisier than those of the other samples are of sufficient quality to trust the results for the shells which were fitted. The differences between samples F-Ac and X-Ac were also evidenced by EELS spectroscopy which indicated that in sample X-Ac the nanoparticles are surrounded by a outer layer of oxide which is not present in sample F-Ac.[37] Even if textural data on the film samples are not available, it is likely that they are denser than the xerogel sample so that the matrix protects the nanoparticles against oxidation. In accordance with this view, EELS results pointed out the presence of void between the nanoparticles and the silica matrix in the xerogel samples which is not present in the film samples.[37]

In all of the reduced samples, the data were interpreted assuming there is no reduction of coordination numbers for high order shells because of the dimensions of the nanoparticles. Even if this possibility cannot be completely ruled out due to the high correlation between coordination numbers and Debye−Waller factors, a significant reduction of coordination numbers for outer shells is not expected,[31] because TEM observations showed that the average dimensions of the nanoparticles in the reduced samples is around 10 nm.[12,13]

As previously observed in $NiO-SiO_2$ and $Fe_2O_3-SiO_2$,[15,16] it seems that the FeCo nanoparticles are not tightly bonded to the silica matrix particles but they are simply embedded in the pores of the network because no evidence of silicon atoms was found in the second neighbor correlations.

Conclusions

Detailed information was obtained on the structural evolution during the sol−gel preparation of $FeCo-SiO_2$ nanocomposites making use of the selectivity of the X-ray absorption techniques which allow us to study separately the Fe and Co environment. Depending on the iron and cobalt precursors used in the sol−gel process, different intermediate products are formed. Nitrate precursors give rise to the formation of ferrihydrite and Co_3O_4, whereas cobalt ferrite is obtained starting from acetate precursors. The reduction treatment of the microporous aerogel obtained starting from nitrate gives rise to the alloy nanoparticles of the desired composition, whereas the mesoporous aerogel, also prepared from nitrate precursors, contains some unalloyed fcc Co. Similar results are also obtained in the xerogel sample obtained starting from nitrate precursors, but in this case, some iron is still in the oxidized form. The reduction of the film, which was obtained from acetate precursors, gives rise to a nanocomposite where practically all of the iron and cobalt atoms are in the bcc FeCo alloy. In the case of the xerogel sample, the same acetate precursors give rise to a sample where a fraction of the iron is still oxidized and some unalloyed cobalt is present.

References and Notes

(1) Gleiter, H. *J. Appl. Crystallogr.* **1991**, *24*, 79.

(2) Siegel, R. W. *Nanostruct. Mater.* **1993**, *3*, 1.

(3) Komarmeni, S. *J. Mater. Chem.* **1992**, *2*, 1219.

(4) Newnham, R. E.; McKinstry, S. E.; Ikaua, H. *Mater. Res. Soc. Symp. Proc.* **1990**, *175*, 161.

(5) Gang, X.; Chien, C. L. *Appl. Phys. Lett.* **1987**, *51*, 1280.

(6) Li, X. G.; Murai, T.; Saito, T.; Takahashi S. *J. Magn. Magn. Mater.* **1988**, *190*, 277.

(7) Moreau, C. E.; Caballero, J. A.; Loloee, R.; Pratt, W. P., Jr; Birge, N. O. *J. Appl. Phys.* **2002**, *87*, 6316.

(8) Bardos, D. I. *J. Appl. Phys.* **1969**, *40*, 1371.

(9) Lataifeh, M. S. *J. Phys. Soc. Jpn.* **2000**, *69*, 248.

(10) De, G.; Mattei, G.; Mazzoldi, P.; Sada, C.; Battaglin, G.; Quaranta, A. *Chem. Mater.* **2000**, *12*, 2157.

(11) Brinker, C. J.; Scherer, G. W. *Sol−gel Science*; Academic Press: San Diego, CA, 1990.

(12) Casula, M. F.; Corrias, A.; Paschina, G. *J. Mater. Chem.* **2002**, *12*, 1505.

(13) Ennas, G.; Casula, M. F.; Falqui, A.; Gatteschi, D.; Marongiu, G.; Piccaluga, G.; Sangregorio, C.; Pinna, G. *J. Non-Cryst. Solids* **2001**, *293−295*, 1.

Spectroscopy Study of FeCo−SiO₂ Nanocomposites

J. Phys. Chem. B, Vol. 107, No. 13, 2003 **3039**

(14) Koningsberger, D. C.; Prins, R. *X-ray Absorption. Principles, Applications, Techniques of EXAFS, SEXAFS and XANES*; Wiley: New York, 1988.

(15) Corrias, A.; Mountjoy, G.; Piccaluga, G.; Solinas, S. *J. Phys. Chem. B* **1999**, *103*, 10081.

(16) Corrias, A.; Ennas, G.; Mountjoy, G.; Paschina, G. *Phys. Chem. Chem. Phys.* **2000**, *2*, 1045.

(17) Casula, M. F.; Corrias, A.; Paschina, G. *J. Mater. Res.* **2000**, *15*, 2187.

(18) Casula, M. F.; Corrias, A.; Paschina, G. *J. Non-Cryst. Solids* **2001**, *293−295*, 25.

(19) Casu, M.; Casula, M. F.; Corrias, A.; Paschina, *J. Non-Cryst. Solids* **2003**, *315*, 97.

(20) Lee, J. G.; Park, J. Y.; Oh, Y. J.; Kim, C. S. *J. Appl. Phys.* **1998**, *84*, 2801.

(21) Grunes, L. A. *Phys. Rev. B* **1983**, *27*, 2111

(22) Binsted, N. *EXCURV98: CCLRC Daresbury Laboratory computer program.* 1998.

(23) Gurman, S. J.; Binsted, N.; Ross, I. *J. Phys. C* **1984**, *17*, 143.

(24) Teo, B. K. *J. Am. Chem. Soc.* **1981**, *103*, 3990.

(25) von Barth, U.; Hedin, L. *J. Phys C.* **1972**, *5*, 1629.

(26) Crozier, E. D. *Nucl. Instr. Method Phys. Res. B* **1997**, *133*, 134.

(27) Bianconi, A. *X-ray absorption: principles, applications, techniques of EXAFS, SEXAFS and XANES*; Koninbsberger, D. C., Prins, R., Eds; Wiley: New York, 1987; Chapter 11.

(28) Drits, V. A.; Sakharov, B. A.; Salyn, A. L.; Manceau, A. *Clay Minerals* **1993**, *28*, 185.

(29) Inoue T. J. *Electrochem. Soc. Jpn.* **1955**, *23*, 24.

(30) Smith, W. L.; Hobson, A. D. *Acta Crystallogr. B* **1973**, *29*, 362.

(31) Greegor, R. B.; Lytle, F. W. *J. Catal.* **1980**, *63*, 476.

(32) Swanson, H. E.; Tafte, E. *Natl. Bur. Stand. (US), Circ.* **1955**, *539*, 4.

(33) Owen, E. A.; Madoc Jones, D. *Proc. Phys. Soc.* **1954**, *67*, 459.

(34) Rehr, J. J.; Albers, R. C. *Phys. Rev. B* **1990**, *41*, 8139.

(35) Rehr, J. J.; Albers, R.C.; Zabinsky, S.I. *Phys. Rev. Lett.* **1992**, *69*, 3397.

(36) Livage, J.; Sanchez, C.; Babonneau, F. In *Chemistry of Advanced Materials: An Overview*; Interrante, L. V., Hampden-Smith, M. J., Eds.; Wiley-VCH: New York, 1998.

(37) Falqui, A.; Serin, V.; Calmels, L.; Snoeck, E.; Corrias, A.; Ennas, G. *J. Electron Microsc.* in press.